Auto-ignition based synthesis of Y 2 O 3 for photo-and thermo-luminescent applications

ARTICLE *in* JOURNAL OF ALLOYS AND COMPOUNDS · SEPTEMBER 2013

Impact Factor: 3 · DOI: 10.1016/j.jallcom.2013.09.037

7 AUTHORS, INCLUDING:

R.Hari Krishna
M.S. Ramaiah Institute of Technology
27 PUBLICATIONS **144** CITATIONS
SEE PROFILE

Rps Chakradhar
National Aerospace Laboratories
189 PUBLICATIONS **2,304** CITATIONS
SEE PROFILE

C. Shivakumara
Indian Institute of Science
175 PUBLICATIONS **2,209** CITATIONS
SEE PROFILE

Tiju Thomas
Indian Institute of Science
21 PUBLICATIONS **110** CITATIONS
SEE PROFILE

Journal of Alloys and Compounds 585 (2014) 129–137

Contents lists available at ScienceDirect

Journal of Alloys and Compounds

journal homepage: www.elsevier.com/locate/jalcom

Auto-ignition based synthesis of Y_2O_3 for photo- and thermo-luminescent applications

R. Hari Krishna [a,b,*], B.M. Nagabhushana [b,*], H. Nagabhushana [c], R.P.S. Chakradhar [d], R. Sivaramakrishna [e], C. Shivakumara [f], Tiju Thomas [g]

[a] Department of Chemistry, M.S. Ramaiah Institute of Technology, Bangalore 560 054, India
[b] Visvesvaraya Technological University, Belgaum 590 018, India
[c] Prof. C.N.R. Rao Centre for Advanced Material Science, Tumkur University, Tumkur 572 103, India
[d] CSIR-National Aerospace Laboratories, Bangalore 560017, India
[e] Department of Chemistry, REVA Independent PU college, Bangalore 560 024, India
[f] Solid State and Structural Chemistry Unit, Indian Institute of Science, Bangalore 560 012, India
[g] Materials Research Centre, Indian Institute of Science, Bangalore 560 012, India

ARTICLE INFO

Article history:
Received 18 June 2013
Received in revised form 19 August 2013
Accepted 5 September 2013
Available online 21 September 2013

Keywords:
Nanophosphor
Y_2O_3
Solution combustion
Photoluminescence
Thermoluminescence

ABSTRACT

We present a simple route for synthesis of Y_2O_3 for both photoluminescent (PL) and thermoluminescent (TL) applications. We show that by simply switching the fuel from ethylene di-amine tetracetic acid (EDTA) to its disodium derivative (Na_2-EDTA), we obtain a better photoluminescent material. On the other hand, use of EDTA aids in formation of Y_2O_3 which is a better thermoluminescent material. In both cases pure cubic nano-Y_2O_3 is obtained. For both the material systems, structural characterization, photoluminescence, thermoluminescence, and absorbance spectra are reported and analyzed. Use of EDTA results in nano Y_2O_3 with crystallite size ~10 nm. Crystallinity improves, and crystallite size is larger (~30 nm) when Na_2-EDTA is used. TL response of Y_2O_3 nanophosphors prepared by both fuels is examined using UV radiation. Samples prepared with EDTA show well resolved glow curve at 140 °C, while samples prepared with Na_2-EDTA shows a glow curve at 155 °C. Effect of UV exposure time on TL characteristics is investigated. The TL kinetic parameters are also calculated using glow curve shape method. Results indicate that the TL behavior of both the samples follow a second order kinetic model.

1. Introduction

Rare earth oxides (REO) have been extensively studied in recent years due to their unique electronic, optical, and chemical properties, which in turn enables their use in several engineering applications [1,2]. Among REO, Y_2O_3 has gained significant attention owing to its use as a dielectric insulator in complementary metal oxide semiconductor (MOS) devices. Its wide energy band gap (~5.5 eV) along with its relatively high dielectric constant, chemical stability, and thermal stability (melting point ~ 2325 °C) makes it a robust engineering material [3]. Furthermore, Y_2O_3 is an important material for optical applications because of its ability to host rare earth atoms [4,5]. In fact many of the best red phosphors used in fluorescent lamps and flat panel devices are Y_2O_3 based systems [6–8].

A wide variety of processes are available for the synthesis of REO. Y_2O_3 powder has been synthesized by various wet chemical routes, such as co-precipitation [9], hydrothermal [10], sol–gel [11] gas-phase condensation [12] and solution combustion [13,14] route. With appropriate processing parameters, these wet chemical processes result in nano-sized powders with narrow particle size distribution. Among the synthesis processes explored so far, the solution combustion method has the advantage of being rapid and low in cost. Another advantage of this method is that the desired phase can be achieved with better control over stoichiometry with a relatively simple experimental setup. In solution combustion method, the desired product is obtained through a self-sustaining exothermic redox reaction, which takes place in a gel that is formed by dehydrating an aqueous solution of a fuel (e.g. polycarboxilic acid) and an oxidant (e.g. metal nitrates). Powder characteristics like crystallite size, surface area, extent and nature (hard or soft) of agglomeration are primarily governed by enthalpy or flame temperature generated during combustion, which itself is dependent on nature of the fuel, fuel-to-oxidant ratio, and amount of gaseous byproducts [15].

* Corresponding authors. Tel.: +91 9916030272 (B.M. Nagabhushana), +91 9886434109 (R. Hari Krishna).
E-mail addresses: rhk.chem@gmail.com (R. Hari Krishna), bmnshan@yahoo.com (B.M. Nagabhushana).

0925-8388/$ - see front matter © 2013 Elsevier B.V. All rights reserved.
http://dx.doi.org/10.1016/j.jallcom.2013.09.037

The choice of fuel significantly impacts the exothermicity and amount of gases that evolve during the combustion process; this in turn has a strong influence on the properties of the product [16]. The fuels employed so far in the combustion synthesis of Y_2O_3 are glycine [17], citric acid [18], urea [19], oxalyldihydrazide [20], carbohydrazide [21], etc. Complexing ability is one of the primary characteristics that a fuel should possess. Among the complexing agents, EDTA and Na_2-EDTA are known to be particularly efficient due to the presence of amine groups in these molecules. Such molecules can effectively complex metal ions of different sizes, and help in achieving chemical homogeneity in the end products. However the high chelating abilities of EDTA and Na_2-EDTA has not been widely used as a fuel in solution combustion reactions.

In the present work, we prepare nano-Y_2O_3 powder by combustion technique using both EDTA and Na_2-EDTA. The combustion synthesized powders are characterized using powder X-ray diffraction (PXRD), Fourier Transform Infrared (FTIR) spectroscopy, UV–Vis spectroscopy, Brunauer–Emmett–Teller (BET) specific surface area analysis, scanning electron microscopy (SEM) and transmission electron microscopy (TEM). We show that by simply switching the fuel from EDTA to its disodium derivative (i.e. Na_2-EDTA) we obtain a better photoluminescent material. On the other hand, use of EDTA aids in formation of Y_2O_3 that is thermoluminescent.

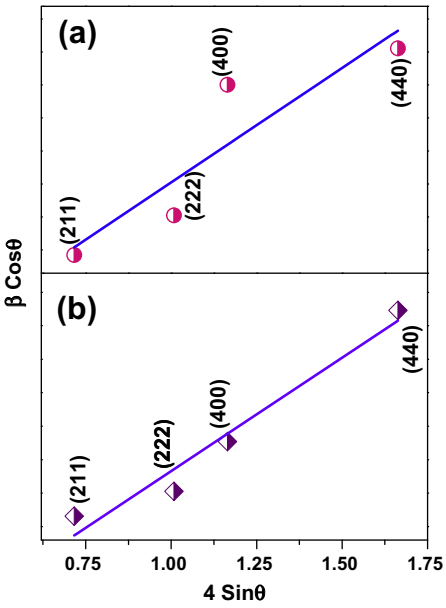

Fig. 2. Williamson–Hall plots of (a) EDTA Y_2O_3 (b) Na_2-EDTA Y_2O_3. The scatter around the linear fit indicates the presence of lattice strains in these nanoparticles.

2. Experimental

2.1. Chemicals

Analytic grade yttrium oxide (Y_2O_3: 99.99%, CDH Ltd.), nitric acid (HNO_3: 99.99%, Merk Ltd.) EDTA ($C_{10}H_{16}N_2O_8$: 99.99%, Merk Ltd.) and Na_2-EDTA ($C_{10}H_{14}N_2O_8Na_2$: 99.99%, Merk Ltd.) are used as starting materials for the preparation of Y_2O_3 nanoparticles. All the chemicals are used without further purification.

2.2. Synthesis

Yttrium oxide is dissolved in 1:1 nitric acid and heated in a sand bath at 80 °C to get transparent, highly viscous yttrium nitrate gel. The excess nitric acid is evaporated. EDTA is dissolved in deionized water, and the solution is subsequently dropped into the yttrium nitrate solution. Continuous stirring is done to ensure homogeneity of the solution. The petri dish containing the homogeneous mixture of yttrium nitrate and EDTA is placed in a pre-heated muffle furnace which is maintained at 500 ± 10 °C. Initially the solution boils and undergoes dehydration, which is followed by decomposition accompanied by evolution of large amounts of gases (oxides of carbon and nitrogen). This is followed by spontaneous smoldering type combustion with enormous swelling of the reaction mixture, which in turn produces foamy and voluminous Y_2O_3. Same procedure is followed in the preparation of Y_2O_3 with disodium salt of EDTA as fuel. The theoretical equations (F/O = 1.0) for the formation of Y_2O_3 nanoparticles using different fuels can be represented by the following reactions:

$$\text{EDTA}: 8Y(NO_3)_3 + 3C_{10}H_{16}N_2O_8 \rightarrow 4Y_2O_3 + 30CO_2 + 15N_2 + 24H_2O, \sim 17 \text{ moles of gases/mol of } Y_2O_3 \quad (1)$$

$$\text{Na}_2\text{-EDTA}: 10Y(NO_3)_3 + 3C_{10}H_{14}N_2O_8Na_2 \rightarrow 5Y_2O_3 + 6NaNO_3 + 30CO_2 + 15N_2 + 21H_2O, \sim 13 \text{ moles of gases/mol of } Y_2O_3 \quad (2)$$

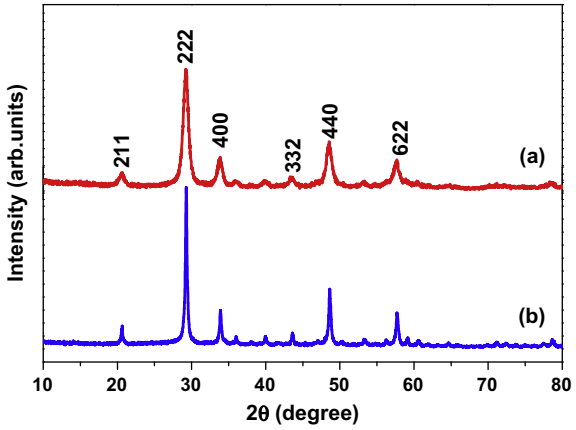

Fig. 1. X-ray diffraction patterns of Y_2O_3 samples synthesized using (a) EDTA and (b) Na_2-EDTA as fuels. (Samples are labeled as EDTA Y_2O_3 and Na_2-EDTA Y_2O_3 respectively.)

2.3. Characterization

The phase purity and crystallinity of the nanophosphors are examined by powder X-ray diffractometer (PANalytical X'Pert Pro) using Cu Kα (1.541 Å) radiation with a nickel filter. The surface morphology of the product is examined using an SEM (JEOL JSM 840A). A Quanta Chrome Corporation NOVA 1000 gas sorption analyzer is used to find the surface area of the powder samples using the BET approach. Transmission electron microscopy (TEM) analysis is performed on a Hitachi H-8100 (accelerating voltage up to 200 kV, LaB_6 filament) equipped with EDS (Kevex Sigma TM Quasar, USA).

The FT-IR studies are performed on a Perkin Elmer Spectrometer (Spectrum 1000) with KBr pellets. The UV–Vis absorption of the samples is recorded on SL 159 ELICO UV–Vis Spectrophotometer. The photoluminescence (PL) measurements are performed on a Jobin Yvon spectrofluorimeter (Fluorolog–3) equipped with a 450-W xenon lamp as an excitation source. This instrument comes with a sample holder that ensures that the sample thickness is uniform throughout. This in turn ensures that the sample area exposed to excitation source, and the distance between the sample and the detector is kept the same for all the measurements. This is how we were able to compare the PL intensities of different samples. TL measurements are carried out at room temperature using Nucleonix TL reader, using UV-irradiation (250 nm wavelength) as excitation with irradiation time in the range 20–140 min.

Table 1
Estimated crystallite size and strain of Y_2O_3 nanoparticles prepared using EDTA and Na_2-EDTA fuels.

System	Crystallite Size (nm)		Band Gap (eV)	Strain ($\times 10^{-4}$)
	Scherer's (nm)	W–H plots (nm)		
EDTA-Y_2O_3	10	11	4.8	14.00
Na_2EDTA-Y_2O_3	30	32	5.2	5.00

Fig 1a and b represents the XRD patterns of the products obtained using EDTA and Na_2-EDTA fuels respectively. The two products are labelled as EDTA Y_2O_3 and Na_2-EDTA Y_2O_3 henceforth. XRD patterns for both the samples show peaks corresponding to all the planes of standard cubic phase Y_2O_3 (JCPDS 70-0134). Diffraction pattern for EDTA Y_2O_3 shows broad and unresolved XRD lines, whereas XRD pattern for Na_2-EDTA Y_2O_3 sample show crystalline and well resolved peaks. This difference in crystallinity of samples with change in fuel may be due to the difference in the number of moles of gases evolved during combustion.

The average crystallite size (D) of Y_2O_3 samples for different fuels are estimated from the full width at half maximum (FWHM) of the (222) diffraction peak of the powders. This is done using the Scherrer formula [22]. From the observed XRD patterns, it is evident that tensile lattice strain is different for samples prepared using different fuels. To quantify this correlation, we followed a method suggested by Williamson and Hall (W–H) [23]. The W–H method is applicable in cases where both crystallite size effect and lattice deformation are simultaneously operative. The combined effect of size effect and lattice deformation gives rise to the observed FWHM (β) in the XRD patterns. β is the sum of $\beta 1$ (grain size dependent broadening) and $\beta 2$ (lattice distortion dependent broadening). This relation assumes a negligibly small instrumental contribution compared to the sample-dependent broadening. W–H equation may be expressed in the form:

$$\beta \cos\theta = \varepsilon(4 \sin\theta) + \frac{\lambda}{D} \quad (3)$$

where β (FWHM in radian), ε is the strain developed and D is the grain size. The equation represents a straight line between $4 \sin\theta$ (X-axis) and $\beta \cos\theta$ (Y-axis), where 2θ is the Bragg angle corresponding to XRD peaks. The slope of line gives the strain (ε) and intercept (λ/D) of this line on the Y-axis gives grain size (D). Fig. 2 shows W–H plot for Y_2O_3 nanopowders prepared with different fuels. It is observed from W–H plot that a good linear fit is not observed. This is due to the intrinsic lattice strains (Table 1) present in nanoparticles owing to their large surface to volume ratio. This is consistent with the previous studies on similar nanoparticles [24,25].

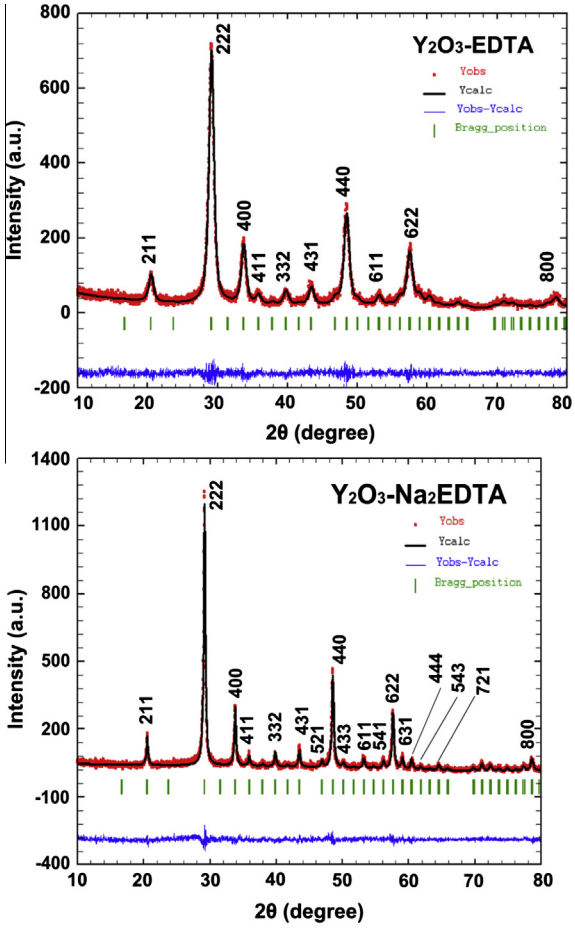

Fig. 3. Reitveld refinement of cubic Y_2O_3 nanoparticles prepared by EDTA and Na_2-EDTA. All the observed peaks are fitted (with statistical validity $R_{Bragg} = 2.3$) and indexed using JCPDS 70-0134.

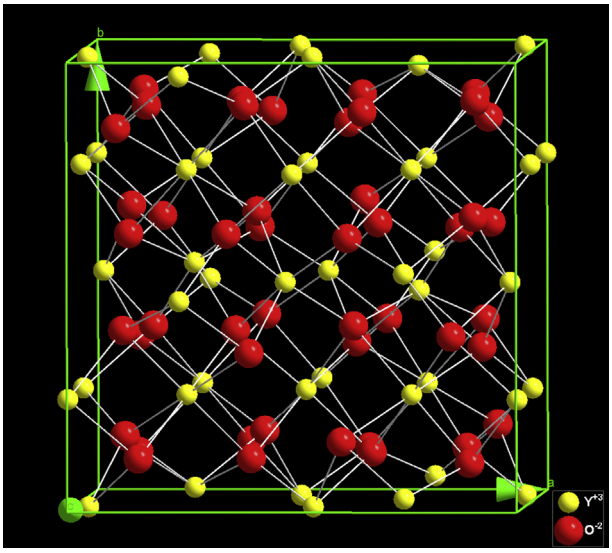

Fig. 4. Packing diagram of cubic Na_2-EDTA Y_2O_3.

The crystallite sizes of the powders as determined from Scherrer's formula and W–H method are summarized in Table 1. Lowest crystallite size is observed for sample prepared using EDTA fuel due to amorphous nature of the product. It is interesting to notice that crystallinity and crystallite size increases for sample prepared using Na_2-EDTA fuel. This is attributed to the presence of sodium ions in Na_2-EDTA sample, which could result in formation of molten $NaNO_3$ flux. This in turn helps in homogeneous mixing of reactants and uniform distribution of reactant ions that chelate with the fuel, which results in the uniform and homogeneous combustion reaction. Molten $NaNO_3$ formed in situ is hence expected to result in particles with improved crystallization and increased size. This is reasonable since Manjunatha et al. [26] recently studied the effect of NaF flux on microstructure of $CdSiO_3$. In their study they showed that the addition of NaF significantly improves the crystallinity of the $CdSiO_3$:Sm^{3+} phosphor.

From the X-ray line broadening data, we notice that the diffraction peaks become broader for EDTA Y_2O_3. The observed increase in FWHM of XRD peaks in this sample is attributed to reduced crystallinity or formation of smaller crystallites in these samples. This is likely due to the fact that the solubility of EDTA is less compared to Na_2-EDTA fuel; this results in less homogeneous combustion with reduced flame temperature. Also the number of moles of gases evolved is more for EDTA fuel than Na_2-EDTA fuel. The reduced temperature coupled with increased gas emission reduces the possibility of local sintering among the primary crystallites, thereby reducing the crystallite growth.

Table 2
Rietveld refined structural parameters of cubic Y_2O_3 nanoparticles prepared using EDTA and Na_2-EDTA as fuels.

Parameters	Fuel	
	EDTA	Na_2-EDTA
Crystal system	Cubic	Cubic
Space group	*Ia3-206*	*Ia3-206*
Lattice parameter	10.632(4) Å	10.612(8) Å
*Y*1	8b	8b
X	−0.0304(3)	−0.0306(3)
Y	0.0000	0.0000
Z	0.2500	0.2500
*Y*2	24d	24d
X	0.2500	0.2500
Y	0.2500	0.2500
Z	0.2500	0.2500
O1	48e	48e
X	0.3911(2)	0.3975(2)
Y	0.1563(2)	0.1515(2)
Z	0.3836(2)	0.3857(2)
R-factors		
R_p	9.0	10.1
R_{wp}	12.4	13.6
R_{Bragg}	2.32	5.92
R_F	2.30	4.60
χ^2	0.804	0.902

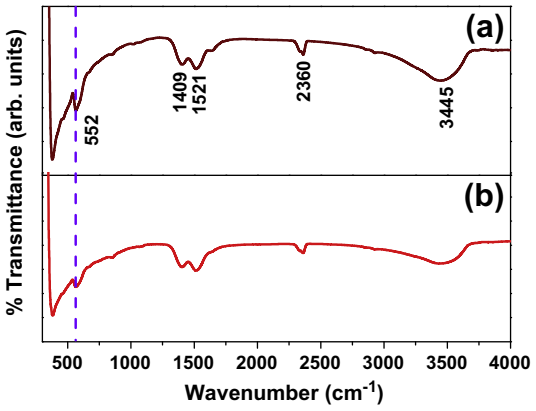

Fig. 5. FTIR spectra of (a) EDTA Y_2O_3 and (b) Na_2-EDTA Y_2O_3.

Rietveld refinement is a method in which various parameters of the XRD pattern (FWHM of peaks, asymmetry of peaks, peak shifts, etc.) can be used to estimate the crystal structure of the material under study. In the present study the Rietveld method is applied mainly for the purpose of evaluating unit cell parameters of the samples. Refinement is done on both EDTA Y_2O_3 and Na_2-EDTA Y_2O_3 (Fig. 3). Rietveld refinement is done using the FULLPROF program [27]. We utilize the pseudo-Voigt function in order to fit parameters to the experimental data set. The parameters used are: a scale factor, a zero shifting factor, four back ground factors, three cell parameters, five shape and width of the peak factors, one global thermal factors and two asymmetric factors. The final refinement analysis shows that the experimental and calculated PXRD patterns obtained by the Rietveld refinement are in good agreement with each other, and all observed peaks have been suitably indexed. For the Rietveld refinement reported, the statistical validity (R_{bragg}) obtained is 2.3, which is well within the permissible limit (~6). The packing diagram of EDTA Y_2O_3 obtained using Rietveld refinement is shown in Fig. 4. The refined parameters such as occupancy and atomic functional positions of the Y_2O_3 nanoparticles are summarized in Table 2. The fitting parameters (R_p, R_{wp} and χ^2) indicate good agreement between the refined and observed PXRD patterns for the Y_2O_3 nanoparticles.

The phase formation and purity of the products are further confirmed by FTIR spectroscopy, and results are shown in Fig. 5a and b. The strong absorption peak ~552 cm^{-1} is ascribed to the stretching vibration of the Y–O bond [28]. The absorption bands in the range 1400–1600 cm^{-1} are ascribed to the bond stretching mode of CO_3^{2-}. Presence of CO_3^{2-} is due to the organic precursors which are used as fuel. The absorption peak at 3445 cm^{-1} is due to O–H stretching vibration of H_2O [29]. This is typical of most of nanomaterials, since their high specific areas results in significant adsorption of atmospheric water vapor. It is also worth noticing a band at ~2360 cm^{-1} corresponding to nitrate group (NO_3^-). These residual nitrates come from the starting nitrate precursors used. No noticeable difference is seen between the FTIR spectra of the samples prepared with different fuels. Like the PXRD results discussed earlier, FT-IR studies further confirms the formation of pure Y_2O_3 product with no other major impurities or secondary phases.

The scanning electron micrographs of EDTA Y_2O_3 and Na_2-EDTA Y_2O_3 are shown in Fig. 6a and c respectively. EDTA Y_2O_3 exhibits highly porous structure with loosely distributed fine particles on the surface. This may be due to the reduced solubility of EDTA (when compared to Na_2-EDTA), and the reduced flame temperature that inhibits partial sintering of particles during synthesis. Micrographs of the Na_2-EDTA Y_2O_3 show porous and foamy large aggregates. This sample has a disconnected structure, and has large voids. Na_2-EDTA fuel has a much higher solubility in water. When this fuel is used, $NaNO_3$ is expected to act as an in situ flux, which results in highly homogeneous combustion. This results in higher flame temperature, which leads to partial sintering of particles. This is the likely reason for the significant agglomeration observed in this sample. Fig. 6b and d shows TEM images of Y_2O_3 powders obtained using EDTA and Na_2-EDTA respectively. TEM shows that nanopowders obtained with EDTA show porous frame with a significant amount of the amorphous phase. The particles in this case are in the range ~10 nm. On the other hand, Na_2-EDTA Y_2O_3 exhibits highly agglomerated particles with sizes in the range ~30 nm. These results are consistent with SEM and XRD results.

Specific surface area (SSA) is one of the essential material parameters in nanopowders. The surface area (m^2/g) of powder samples is dependent on many parameters such as particle size, shape, surface textures, and size distribution. Porosity is also a crucial factor that determines the SSA. Combustion-derived products usually exhibit good SSA since the release of heat (exothermicity) during the combustion reaction is long enough for nucleus formation, but too short for grain growth [30]. The surface area and pore size distribution of the samples prepared using EDTA and Na_2-EDTA is determined from the corresponding nitrogen adsorption and desorption isotherms, and are presented in Figs. 7a and Figs. 7b respectively. The BET surface area of Y_2O_3 powders prepared with EDTA and Na_2-EDTA are 27.00 and 20.00 m^2/g respectively (Table 3). The higher surface area for sample

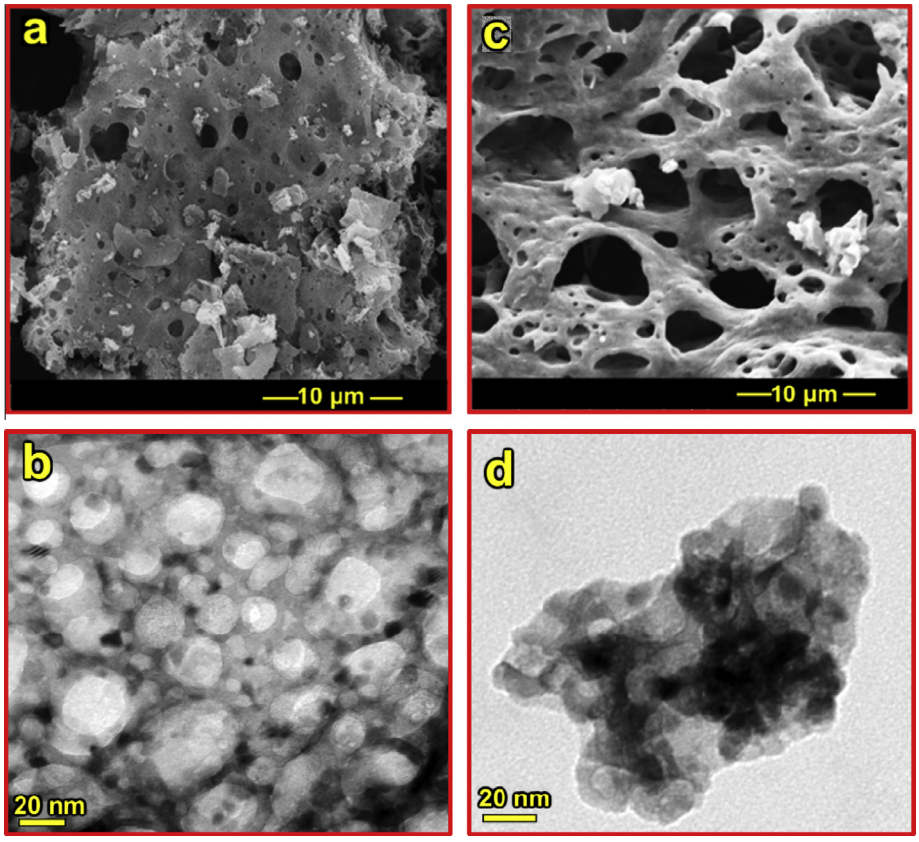

Fig. 6. Scanning electron micrographs (SEM) and transmission electron micrographs (TEM) of EDTA Y_2O_3 (a and b) and Na_2-EDTA Y_2O_3 (c and d).

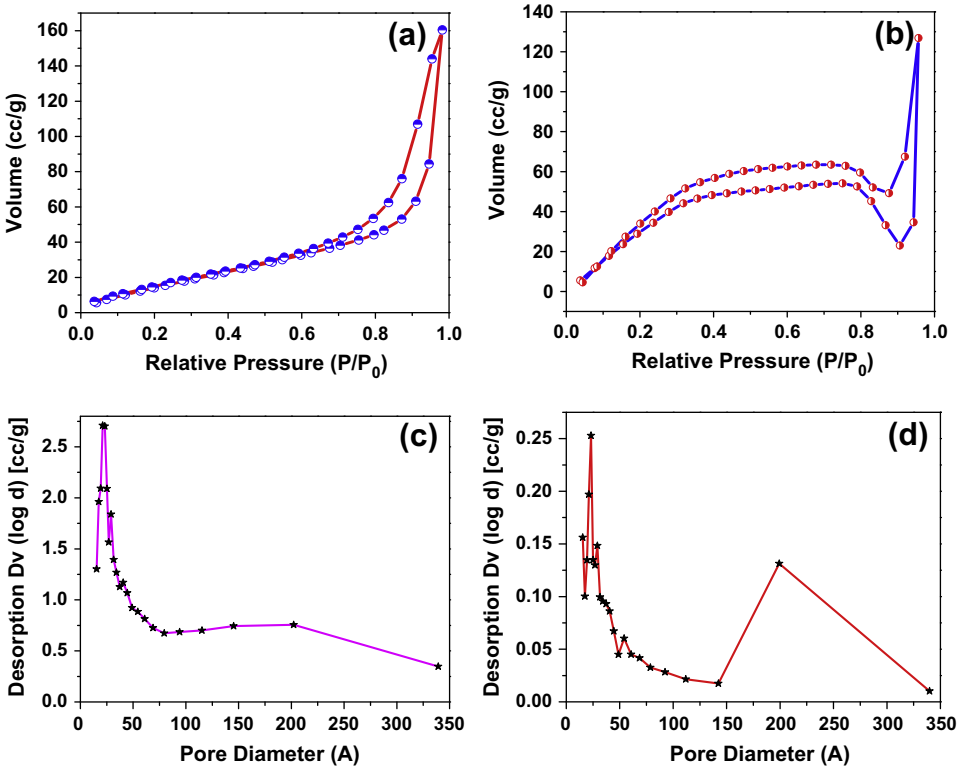

Fig. 7. Nitrogen adsorption/desorption isotherms of (a) EDTA Y_2O_3, (b) Na_2-EDTA Y_2O_3. The pore size distribution of (c) EDTA Y_2O_3 and (d) Na_2-EDTA Y_2O_3 particles is obtained through the Barrett-Joyner-Halenda method.

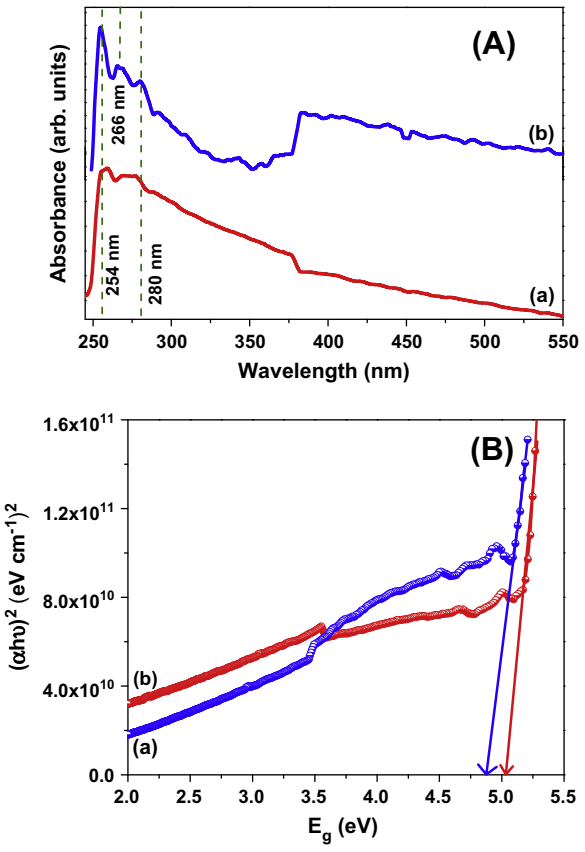

Fig. 8. (A) UV–Vis absorption spectra, and (B) optical energy band gap of (a) EDTA Y_2O_3, (b) Na_2-EDTA Y_2O_3.

Table 3
Physical parameters extracted of Y_2O_3 nanoparticles prepared using different fuels. The parameters are obtained using Brunauer–Emmett–Teller analysis.

System	Surface area (m^2/g)	Pore volume (V) (cm^3/g)	Pore diameter (Å)
EDTA-Y_2O_3	27.00	0.223	33.5
Na_2-EDTA-Y_2O_3	20.00	0.196	37.8

prepared with EDTA is due to reduced flame temperature which results in reduced crystallite size. The reason for this has been discussed above. Likewise decrease in surface area for powder prepared using Na_2-EDTA sample is attributed to more homogeneous combustion with higher flame temperature which leads to partial sintering of particles.

Fig. 7c and d shows the pore size distribution which are calculated using the Barrett–Joyner–Halenda (BJH) model. For this calculation, N_2 isotherms are used. The pore size distribution of both the samples show that pore diameter 10–160 Å with a maximum at about 22 Å. The surface area, pore volume and pore diameter for the samples prepared with two different fuels are summarized in Table 3.

UV–Vis spectra of Y_2O_3 nanoparticles prepared by different fuels are shown in Fig. 8 A. Two absorption peaks at ~254 nm (sharp), ~266 and 280 nm (broad) are recorded. The maximum absorption (~254 nm) is due to transition between valence band and conduction band [31]. The weak absorptions (~266 and 280 nm) observed in the UV–Vis region is attributed to transitions involving extrinsic states such as surface traps/defect states/impurities [32]. It is well known that smaller size particles have high surface to volume ratio. This results in increase in defect density. This is also why nanomaterials often exhibit strong and broad absorption bands [33]

The optical band gap energy (E_g) is estimated using Wood and Tauc relation [34] given by:

$$(\alpha h\nu)\alpha(h\nu - E_g)^{1/n} \quad (4)$$

where 'a' is the absorption coefficient, $h\nu$ the photon energy, E_g the energy gap, and $n = 2$ for direct allowed transition. For direct band gap materials, Eq. (4) can be rearranged and written in the form:

$$(\alpha h\nu)^2\alpha(h\nu - E_g) \quad (5)$$

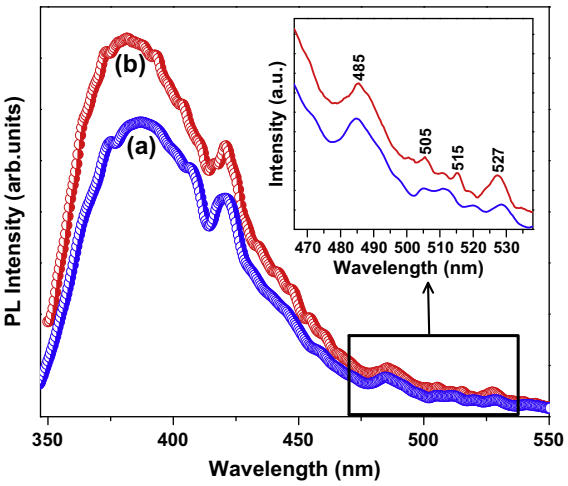

Fig. 9. Photoluminescence (PL) spectra of (a) EDTA Y_2O_3 and (b) Na_2-EDTA Y_2O_3. Oxygen deficiency in Y_2O_3, which occurs due to the carbon rich ambient occurring during the synthesis, plays a crucial role in determining the observed PL.

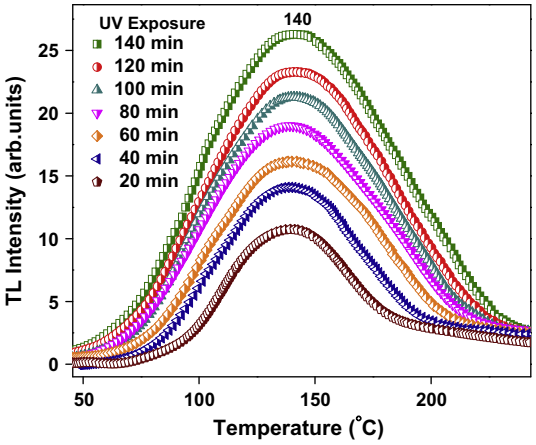

Fig. 10. Thermoluminescence (TL) glow curves of UV-irradiated (20–140 min) EDTA Y_2O_3. This sample shows TL response with good dose linearity.

The energy gap is determined by plotting $(\alpha h\upsilon)^2$ versus $h\upsilon$ and finding the intercept on the $h\nu$ axis, as shown in Fig. 8B. The band gap in sample prepared with EDTA is less (E_g = 4.8 eV) when compared to sample prepared with Na_2-EDTA (E_g = 5.2 eV). The band gap of Na_2-EDTA Y_2O_3 are consistent with the reported band gap of Y_2O_3 [35]. The lower E_g of EDTA Y_2O_3 most likely has to do with the higher structural disorder in its lattice. The optical band gap, E_g values mainly depend on the preparation methods and processing conditions (heat treatment, reaction time, reaction temperature, etc.). Sample prepared with EDTA fuel is slightly amorphous in nature. The structural defects in this system are expected to introduce defect states between valence and conduction band, which would reduce the observed optical band gap. On the other hand, Na_2-EDTA Y_2O_3 is highly crystalline and therefore the concentration of structural defects (oxygen vacancies, distortion or strain in lattice) is minimal; this explains the large E_g (5.2 eV) observed.

Fig. 9a and b shows the photoluminescence spectrum of Y_2O_3 nanophosphors prepared using EDTA and Na_2-EDTA as fuels respectively. Upon 248 nm excitation, a series of emission bands ranging from UV to green region are observed. The bands observed are centered at 380, 421, 485, 505, 515 and 527 nm. Since Y^{3+} itself is non-luminous, the observed luminescence from Y_2O_3 samples must be due to non-stoichiometry created by the oxygen deficiency in the system, which is known to occur when Y_2O_3 forms in carbon rich ambient [36]. Carbon related impurities, caused due to the use of carbon based fuels used in combustion synthesis, contribute to the luminescence of Y_2O_3.

In the emission spectra, the broad emission peak at 380 nm in UV region is attributed to radiative recombination of photo-generated hole with an electron occupying the oxygen vacancy [37]. Emission band centered at 421 nm is attributed to recombination of a delocalized electron close to the conduction band with a single charged state of surface oxygen vacancy [38]. The emission band at 485 nm can

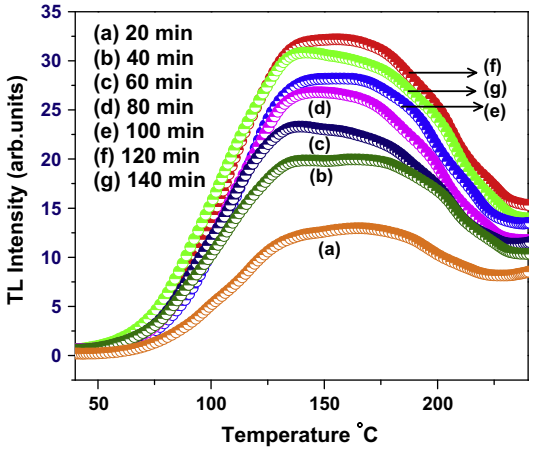

Fig. 11. Thermoluminescence glow curves of UV-irradiated (20–140 min) Y_2O_3 nanoparticles prepared by Na_2-EDTA.

be attributed to self-trapped excitation luminescence [39]. Other weak emission peaks at ~505, 515 and 527 nm are due to different kinds of oxygen vacancies. It is observed that intense and well resolved emission peaks are recorded for Na_2-EDTA Y_2O_3 when compared to EDTA Y_2O_3 fuel. This enhanced photoluminescence response for Na_2-EDTA sample is attributed to better crystallinty of the sample.

Figs. 10 and 11 show TL glow curve characteristics of UV exposed (20–140 min) EDTA Y_2O_3 and Na_2-EDTA Y_2O_3. A broad TL peak at 140 °C is recorded in EDTA Y_2O_3, whereas in the case of Na_2-EDTA Y_2O_3 a broad peak centered at 155 °C is recorded. Heating rate is kept constant (2.5 °C s^{-1}) in both cases. It is clear that the shape and position of TL peaks are almost the same in the dose range studied, showing a dose independent character. However it is apparent the intensities of the TL peaks changes with the increase in the UV exposure time. It is worth noticing that the glow peak is well defined in case of EDTA Y_2O_3 when compared to Na_2-EDTA Y_2O_3.

Variation in TL intensity with different UV exposures is recorded and shown in Fig. 12. The peak heights are used for measuring the TL intensities. In Na_2-EDTA Y_2O_3, TL intensity increases with UV exposure up to 120 min, after which it decreases. This trend is generally due to competition between radiative and non-radiative centers, or between different kinds of trapping centers. However in the case of EDTA Y_2O_3, TL intensity increases with UV exposure. In the present study UV exposure is used for creation of defects, and the observed TL glow peaks is mainly attributed to surface defects, since UV radiation cannot penetrate deep into the material [40]. The sublinear increase in TL intensity with UV exposure can be explained on the basis of Horowitz's TIM (track interaction model) [41,42]. At low exposure time the recombination of various trapping/luminescent centres (TCs/LCs) occurs entirely within the tracks. Electrons escaping the tracks are intercepted by the non-radiative competitive centres (CC) in the intermediate region. The TL signal, therefore, linearly increases with the irradiation and is simply proportional to the UV dose (the exposure time). At higher dosage levels, the distance between neighbouring tracks decreases and the electrons leaving the track reach

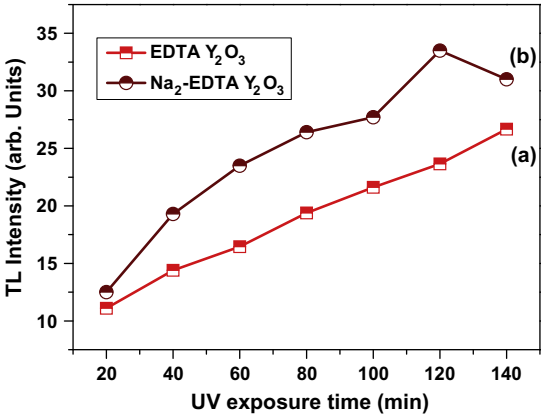

Fig. 12. Variation of Thermoluminescence glow peak intensity with UV-irradiated (20–140 min) (a) EDTA Y_2O_3 and (b) Na_2-EDTA Y_2O_3. EDTA Y_2O_3 shows TL response with better dose linearity.

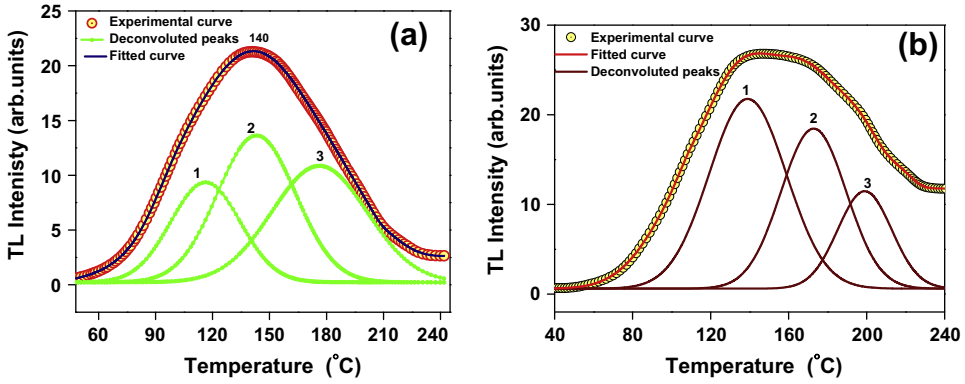

Fig. 13. Glow curve deconvolution of (a) EDTA Y_2O_3 exposed to 100 min of UV radiation and (b) Na_2-EDTA Y_2O_3 exposed to 80 min of UV radiation.

Table 4
Estimated trap parameters of irradiated Y_2O_3 nanoparticles which are prepared using EDTA fuel. UV dose is varied by changing the irradiation time.

UV dose (min)	Peak	T_m (°C)	Order of kinetics b (μ_g)	Activation energy (eV)				Frequency factor, s(Hz)
				E_τ	E_δ	E_ω	E_{ave}	
20	1	106	2(0.51)	0.69	0.72	0.71	0.70	3.34E + 10
	2	144	2(0.51)	0.72	0.76	0.74	0.73	1.05E + 10
	3	186	2(0.48)	1.18	1.20	1.20	1.19	2.38E + 14
40	1	101	2(0.52)	0.86	0.86	0.87	0.86	8.59E + 12
	2	134	2(0.50)	0.91	0.93	0.92	0.92	3.99E + 12
	3	161	2(0.48)	1.59	1.56	1.58	1.58	5.51E + 19
60	1	114	2(0.50)	1.28	1.26	1.28	1.27	1.02E + 18
	2	130	2(0.50)	1.23	1.21	1.23	1.22	4.56E + 16
	3	174	2(0.50)	1.16	1.17	1.17	1.17	2.61E + 14
80	1	112	2(0.52)	1.40	1.34	1.37	1.37	2.64E + 19
	2	134	2(0.49)	1.15	1.16	1.16	1.16	4.89E + 15
	3	175	2(0.51)	1.47	1.43	1.46	1.45	5.37E + 17
100	1	116	2(0.51)	1.03	1.02	1.03	1.03	4.70E + 14
	2	143	2(0.50)	0.95	0.97	0.96	0.96	7.59E + 12
	3	175	2(0.52)	1.00	1.01	1.01	1.00	3.23E + 12
120	1	102	2(0.50)	0.99	0.99	1.00	0.99	5.27E + 14
	2	126	2(0.51)	1.31	1.27	1.29	1.29	5.29E + 17
	3	154	2(0.50)	1.30	1.29	1.30	1.30	5.02E + 16
140	1	91	2(0.52)	1.16	1.12	1.14	1.14	1.72E + 17
	2	119	2(0.52)	1.07	1.04	1.06	1.06	8.59E + 14
	3	152	2(0.50)	0.77	0.81	0.79	0.79	3.07E + 10

the neighbouring tracks, resulting in the increased recombinations, which results in greater TL intensity. In the present study, the TL intensity increases with UV exposure time, since number of particles irradiated increases with exposure time.

TL characterization of the phosphor requires extraction of information regarding trapping parameters such as activation energy (E) of traps, and order of kinetics (b) associated with the glow peaks. Here E is a measure of energy required to eject an electron from the defect center to the conduction band, while s is the rate of electron ejection. The order of kinetics b is a measure of the probability that a free electron gets re-trapped. This re-trapping effect increases with density of empty traps. For estimation of trapping parameters (s and E), we did deconvolution of the TL glow curves using ORIGIN 8.1 software. This is shown in Fig. 13a and b for EDTA Y_2O_3 and Na_2-EDTA Y_2O_3 respectively. The three curves obtained are needed to account for the two weak shoulders, and one dominant maximum observed in the TL curve.

The following empirical formulae are used to estimate trapping parameters using the Chen's peak shape method [43]:

The activation energy (E)

$$E_\alpha = c_\alpha\left(\frac{kT_m^2}{\alpha}\right) - b_\alpha(2kT_m) \tag{6}$$

where $\alpha = \tau$, δ and ω with $\tau = T_m - T_1$, $\delta = T_2 - -T_m$ and $\omega = T_2 - T_1$

$$C_\tau = 1.51 + 3.0(\mu_g - 0.42) \quad C_\delta = 0.976 + 7.3(\mu_g - 0.42) \tag{7}$$

$$C_\omega = 2.52 + 10.2(\mu_g - 0.42) \tag{8}$$

$$b_\tau = 1.58 + 4.2(\mu_g - 0.42) \quad b_\delta = 0\ b_\omega = 1 \tag{9}$$

Frequency factor (s)

Once E and b are known, frequency factor (s) can be evaluated:

$$s = \frac{\beta E}{kT_m^2}\exp\left(\frac{E}{kT_m}\right)[1 + (b-1)\Delta_m]^{-1} \tag{10}$$

where β is the linear heating rate, b the order of kinetics and $\Delta_m = \frac{2kT_m}{E}$.

Order of kinetics

To determine the order of kinetics (b), the form factor or symmetry factor is determined using the following expression:

$$\mu_g = \frac{T_2 - T_m}{T_2 - T_1} \tag{11}$$

This involves calculation of T_1 and T_2. T_1 and T_2 are the temperatures corresponding to half of the maximum intensities on either side of the glow peak maximum temperature (T_m). The nature of the kinetics can be found by the form factor. Theoretically the value of geometrical form factor (μ_g) is close to 0.42 for first order kinetics, and value is 0.52 for second order kinetics.

The estimated kinetic parameters for EDTA Y_2O_3 and Na_2-EDTA Y_2O_3 phosphor are given in Tables 4 and 5 respectively.

EDTA Y_2O_3 showed better TL response with good linearity. It is important to notice that using right kind of fuel it is possible to maximize the TL efficiency, improve sensitivity, and ensure dose linearity for a specific irradiation type. The traps responsible for TL observed in this case are due to oxygen vacancies produced during the fabrication of nanophosphor and/or due to defects produced by irradiation

Table 5
Estimated trap parameters of irradiated Y_2O_3 nanoparticles which are prepared using Na_2-EDTA fuel. UV dose is varied by changing the irradiation time.

UV exposure time (min)	Peak	T_m (°C)	b (μ_g)	Activation energy, E (eV)				Frequency factor, s (Hz)
				E_τ	E_δ	E_ω	E_{ave}	
20	1	138	2(0.49)	1.25	1.24	1.25	1.25	4.88E + 16
	2	162	2(0.49)	1.41	1.39	1.41	1.40	4.31E + 17
	3	187	2(0.51)	1.14	1.14	1.15	1.14	5.78E + 13
40	1	135	2(0.50)	1.06	1.06	1.07	1.06	2.80E + 14
	2	169	2(0.50)	1.40	1.38	1.40	1.39	1.84E + 17
	3	199	2(0.51)	1.74	1.68	1.72	1.72	5.64E + 19
60	1	125	2(0.49)	1.10	1.10	1.11	1.11	2.23E + 15
	2	155	2(0.51)	1.08	1.08	1.08	1.07	9.33E + 13
	3	189	2(0.50)	1.31	1.30	1.31	1.31	3.70E + 15
80	1	139	2(0.50)	0.89	0.92	0.91	0.90	1.92E + 12
	2	173	2(0.48)	1.29	1.30	1.30	1.30	9.14E + 15
	3	199	2(0.49)	1.62	1.59	1.62	1.61	3.80E + 18
100	1	136	2(0.51)	1.32	1.26	1.29	1.29	2.13E + 17
	2	163	2(0.49)	1.37	1.36	1.37	1.37	1.58E + 17
	3	189	2(0.48)	1.16	1.18	1.18	1.17	1.11E + 14
120	1	136	2(0.49)	1.04	1.06	1.06	1.05	1.93E + 14
	2	166	2(0.49)	1.28	1.28	1.29	1.28	1.14E + 16
	3	194	2(0.49)	1.38	1.38	1.39	1.38	1.79E + 16
140	1	132	2(0.51)	0.83	0.85	0.84	0.84	4.84E + 11
	2	169	2(0.51)	1.52	1.47	1.50	1.50	3.03E + 18
	3	190	2(0.50)	2.33	2.21	2.29	2.28	2.26E + 16

exposure [44]. The obtained experimental results shows that the TL characteristics of a material (e.g. efficiency, saturation, sensitivity and dose linearity) depends greatly on the nature of the fuel used in the combustion synthesis.

3. Conclusions

We show that a single experimental parameter, namely the fuel used in solution combustion synthesis, can be changed to obtain Y_2O_3 that is either photoluminescent (PL) or thermoluminescent (TL) active. We demonstrate that by simply switching the fuel from ethylene diamine tetracetic acid (EDTA) to its disodium derivative (Na_2-EDTA), we obtain a better photoluminescent material. On the other hand, use of EDTA aids in formation of Y_2O_3 that is thermoluminescent. EDTA Y_2O_3 is relatively disordered, has a crystallite size ~10 nm, and has a specific surface area of ~27 m^2/g. Crystallinity is better and crystallite size is larger (~30 nm) when Na_2-EDTA is used. The TL kinetic parameters are also calculated using glow curve shape method. Results indicate that the TL glow curves of both samples follows second order kinetic model. The observed PL is due to oxygen deficiencies in Y_2O_3, while the observed TL characteristics (e.g. supra-linearity in the intensity variation with dosage) is understood using Track Interaction Model (TIM). This work shows that appropriate choice of fuel alone can help to achieve significant improvement in the photoluminescence or thermoluminescence response.

Acknowledgement

R.H.K. is grateful to the Management, Principal and HOD Chemistry of M.S. Ramaiah Institute of Technology, Bangalore, for their constant support and encouragement.

References

[1] S. Som, S.K. Sharma, S.P. Lochab, Mater. Res. Bull. 48 (2013) 844–851.
[2] R.V. Yadav, R.K. Verma, G. Kaur, S.B. Rai, Spectrochim. Acta A 103 (2013) 216–221.
[3] P.H. Holloway, T.A. Trottier, B. Abrams, C. Kondoleon, S.L. Jones, J.S. Sebastian, W.J. Thomes, H. Swart, J. Vac. Sci. Technol. B17 (1999) 758–764.
[4] Christopher Waite, Rusty Mann, Anthony L. Diaz, J. Solid State Chem. 198 (2013) 357–363.
[5] R. Hari Krishna, B.M. Nagabhushana, H. Nagabhushana, N. Suriya Murthy, S.C. Sharma, C. Shivakumara, R.P.S. Chakradhar, J. Phys. Chem. C 117 (2013) 1915–1924.
[6] G. Blasse, B.C. Grabmaier, Luminescent Materials, Springer-Verlag, New York, 1994.
[7] G. Blasse, in: A.H. Katai (Ed.), Solid State Luminescence, Chapman and Hall, London, 1993; p 349.
[8] J.W. Wang, Y.M. Chang, H.C. Chang, S.H. Lin, L.C.L. Huang, X.L. Kong, M.W. Kang, Chem. Phys. Lett. 405 (2005) 314–317.
[9] Wenjing Liu, Yuhua Wangn, Mingqi Zhang, Yunxian Zheng, Mater. Lett. 96 (2013) 42–44.
[10] Xue-Mei Zhang, Man-Lian Huang, Zhi-Jun Zhang, Bi-Qiu Liu, Jing-Tai Zhao, Mater. Lett. 68 (2012) 269–272.
[11] Lu Qiang, YingJun Wu, AiHua Li, Yang Wang, Yang Gao, HongYan Peng, Mater. Sci. Eng. B 176 (2011) 1041–1046.
[12] H.J. Eilers, J. Alloys Comp. 474 (2009) 569–572.
[13] Vijay Singh, Vineet Kumar Rai, Benjamin Voss, Markus Haase, R.P.S. Chakradhar, D. Thirupathi Naidu, Sang Hwan Kim, Spectrochim. Acta A 109 (2013) 206–212.
[14] Srirupa.T. Mukherjee, V. Sudarsan, P.U. Sastry, A.K. Patra, A.K. Tyagi, J. Alloys Comp. 519 (2012) 9–14.
[15] Gurvinderjit Singh, V.S. Tiwari, Pragya Tiwari, A.K. Srivastava, P.K. Gupta, J. Alloys Comp. 509 (2011) 4127–4131.
[16] M.A. Aghayan, M.A. Rodríguez, Mater. Sci. Eng. C 32 (2012) 2464–2468.
[17] R.V. Mangalaraja, J. Mouzon, P. Hedstrom, I. Kero, K.V.S. Ramam, Carlos P. Camurri, M. Oden, J. Mater. Process Tech. 208 (2008) 415–422.
[18] Guodong Xia, Shengming Zhou, Junji Zhang, Sumei Wang, Xu Jun, Chem. Lett. 34 (2005) 1166–1167.
[19] Anurag Pandey, Vineet Kumar Rai, Riya Dey, Kaushal Kumar, Mater. Chem. Phys. 139 (2013) 483–488.
[20] S. Ekambaram, K.C. Patil, M. Maaza, J. Alloys Comp. 393 (2005) 81–92.
[21] Fu. Yen Pei, J. Mater. Sci. 42 (2007) 5165–5169.
[22] P. Klug, L.E. Alexander, X-Ray Diffraction Procedure, Wiley, New York, 1954.
[23] G.K. Williamson, W.H. Hall, Acta Metall. 1 (1953) 22–31.
[24] V. Biju, Neena Sugathan, V. Vrinda, S.L. Salini, J. Mater. Sci. 43 (2008) 1175–1179.
[25] K. Bhattacharjee, C.K. Ghosh, M.K. Mitra, G.C. Das, S. Mukherjee, Kalyan Kumar Chattopadhyay, J. Nanopart Res. 13 (2) (2010) 739–750.
[26] C. Manjunatha, B.M. Nagabhushana, D.V. Sunitha, H. Nagabhushana, S.C. Sharma, G.B. Venkatesh, R.P.S. Chakradhar, J. Lumin. 134 (2013) 432–440.
[27] Rodrigueg-carvajal, J. FULLPROF 2000: a program for Rietveld, profile matching and integrated intensity refinements for X-ray and neutron data, version 1.6; Laboratorie Leon, Brillounin, Gifsuryvette, France, 2009.
[28] S. Som, S.K. Sharma, J. Phys. D: Appl. Phys. 45 (2012) 415102–415108.
[29] Haiming Qin, Hong Liu, Yuanhua Sang, Yaohui Lv, Xiaolin Zhang, Yuanyuan Zhang, Tadashi Ohachi, Jiyang Wang, CrystEngComm 14 (2012) 1783–1789.
[30] B.M. Nagabhushana, R.P.S. Chakradhar, K.P. Ramesh, V. Prasad, C. Shivakumara, G.T. Chandrappa, Philos. Mag. 90 (2010) 2009–2025.
[31] L.K. Pan, Q. Sunchang, C.M. Li, J. Phys. Chem. B 108 (2004) 3404–3406.
[32] H.Q. Cao, X.Q. Qiu, B. Luo, Y. Liang, Y.H. Zhang, R.Q. Tan, M.J. Zhao, Q.M. Zhu, Adv. Funct. Mater. 14 (2004) 243–246.

[33] A. Emeline, G.V. Kataeva, A.S. Litke, A.V. Rudakova, V.K. Ryabchuk, N. Serpone, Langmuir 14 (1998) 5011–5022.
[34] J. Tauc, in: F. Abeles (Ed.), Optical Properties of Solids, North-Holland, Amsterdam, The Netherlands, 1970.
[35] B.N. Lakshminarasappa, J.R. Jayaramaiah, B.M. Nagabhushana, Powder Technol. 217 (2012) 7–10.
[36] E. Kowsari, G. Faraghi, Mater. Res. Bull. 45 (2010) 939–945.
[37] B. Umesha, B. Eraiah, H. Nagabhushana, B.M. Nagabhushana, G. Nagaraja, C. Shivakumara, R.P.S. Chakradhar, J. Alloys Comp. 509 (2011) 1146–1151.
[38] C. Hu, H. Liu, W. Dong, Y. Zhang, G. Bao, C. Lao, Z.L. Wang, Adv. Mater. 19 (2007) 470–474.
[39] Y. Zhang, K. Han, T. Cheng, Z. Fang, Inorg. Chem. 46 (2007) 4713–4717.
[40] M. Chandrasekhar, D.V. Sunitha, N. Dhananjaya, H. Nagabhushana, S.C. Sharma, B.M. Nagabhushana, C. Shivakumara, R.P.S. Chakradhar, J. Lumin. 132 (2012) 1798–1806.
[41] Y.S. Horowitz, O. Avila, M. Rodriguez-Villafuerte, Nucl. Instr. Method. Phys. Res. B 184 (2001) 85–112.
[42] Y.S. Horowitz, M. Rosenkrantz, S. Mahajana, D. Yosian, J. Phys. D: Appl. Phys. 9 (1995) 205–211.
[43] R. Chen, Y. Kirish, Analysis of Thermally Stimulated Processes, Pergamon, New York, 1981.
[44] E. De la Rosa, R.A. Rodrıguez, R. Melendrez, P. Salas, L.A. Diaz-Torres, M. Barboza-Flores, Nucl. Instr. Meth. Phys. Res. B 255 (2007) 357–364.